CARDIFF UNIVERSITY
PRIFYSGOL CAERDYDD

ORCA – Online Research @ Cardiff

This is an Open Access document downloaded from ORCA, Cardiff University's institutional repository:https://orca.cardiff.ac.uk/id/eprint/185300/

This is the author's version of a work that was submitted to / accepted for publication.

Citation for final published version:

Liang, Chen, Zhang, Yanjie, Wang, Xu, Zhu, Hanxing , Lai, Weizhong and Zhang, Hengzhen 2026. Laboratory investigation of breakage and deformation characteristics of phyllite residual fills under varying gradation conditions. Granular Matter 28 , 33. 10.1007/s10035-025-01606-8

Publishers page: https://doi.org/10.1007/s10035-025-01606-8

Please note:
Changes made as a result of publishing processes such as copy-editing, formatting and page numbers may not be reflected in this version. For the definitive version of this publication, please refer to the published source. You are advised to consult the publisher's version if you wish to cite this paper.

This version is being made available in accordance with publisher policies. See http://orca.cf.ac.uk/policies.html for usage policies. Copyright and moral rights for publications made available in ORCA are retained by the copyright holders.

Laboratory Investigation of Breakage and Deformation Characteristics of Phyllite Residual Fills under Varying Gradation Conditions

Chen Liang[1]; Yanjie Zhang[2]; Xu Wang[3]; Hanxing Zhu[4]; Weizhong Lai[5] and Hengzhen Zhang[6]

[1] *Graduate Student, School of Civil Engineering, Lanzhou Jiaotong Univ., Lanzhou 730070, China. Email: 13848722561@163.com*

[2] *Professor, School of Civil Engineering, Lanzhou Jiaotong Univ., Lan-zhou 730070, China (corresponding author). ORCID: https://orcid.org/0000-0002-9969-377X. Email: zhangyanjie@lzjtu.edu.cn*

[3] *National and Provincial Joint Engineering Laboratory of Road and Bridge Disaster Prevention and Control, Lanzhou Jiaotong Univ., Lanzhou 730070, China. Email: publicwang@163.com*

[4] *Reader, School of Engineering, Cardiff Univ., Cardiff CF24 3AA, UK.ORCID: https://orcid.org/0000-0002-3209-6831. Email: ZhuH3@cardiff.ac.uk*

[5] *Engineer,Guoneng Ganquan Railway Co., Ltd., Bayannur 015323, China. Em ail:1604171170@qq.com*

[6] *Undergraduate Student, School of Civil Engineering, Lanzhou Jiaotong Univer sity,Lanzhou 730070, China. Email: 1762904339@qq.com*

Abstract: To elucidate the coupled breakage–deformation mechanisms of soft rock residuals in large-scale embankment applications, this study focuses on phyllite materials from the Kangluo Expressway project in Gansu Province, China. A combined

conditions to examine interactions between particle breakage and deformation. Talbot continuous gradation curves (n = 0.30, 0.50, 0.7) and corresponding single-sized gradations were evaluated. A total of 400 single-particle crushing tests were performed to derive the Weibull modulus *m* and characteristic strength σ_0 through statistical fitting. One-dimensional confined compression tests were then conducted in a steel cylinder (150 mm diameter, 300 mm height) under axial stresses from 0 to 15 MPa to quantify the breakage ratio. In the numerical analysis, a Fragment Replacement Method (FRM) was implemented within the PFC3D discrete element framework. When the octahedral shear stress exceeded a fracture threshold, the mother particle was replaced by 14 Apollonian sub-particles, with conservation of mass and momentum strictly enforced. The simulation results aligned closely with experimental data regarding stress–strain behavior and the correlation between Talbot gradation and breakage ratio. These findings provide experimental validation and theoretical guidance for utilizing soft rock waste and calibrating discrete element models.

Keywords: phyllite waste; particle breakage; continuous gradation; particle breakage rate; fragment-replacement discrete-element method

1 Introduction

Large-scale infrastructure development projects, such as tunnel excavation and road cutting, often generate substantial volumes of soft rock waste. Taking the Kangluo Expressway in Gansu Province as a representative case, the majority of the excavated

materials—from both hillside cuttings and tunnel blasting—consist of phyllite, a low-grade metamorphic rock characterized by pronounced foliation. If disposed of without treatment, such materials not only occupy valuable land resources and pose environmental risks, but also represent a considerable underutilization of potentially recyclable geomaterials. However, soft rock particles are inherently prone to crushing under load, which may lead to excessive post-construction settlement, strength degradation, and reduced permeability in embankment fills—factors that currently constrain their widespread engineering application.

The mechanical strength of granular materials is a fundamental property distinguishing them from continuum media. Understanding the statistical distribution of particle strength is essential for accurately modeling breakage processes and optimizing fill design in geotechnical, transportation, and materials engineering. Early foundational studies by Hiramatsu and Oka (1966), Nakata et al. (1999), and others proposed theoretical expressions for single-particle crushing strength based on uniaxial compression and tension tests, establishing the basis for subsequent research on breakage modeling. Given the prevalence of microcracks and structural defects in granular media, particle failure is inherently stochastic and exhibits significant statistical heterogeneity. The Weibull distribution has been widely employed to describe the nonlinear relationship between particle size and strength. Experimental work by McDowell and Bolton (1998), Lim and McDowell (2005), and Ovalle et al. (2015) validated the applicability of the Weibull model in both single-particle and full gradation compression tests, and emphasized the influence of mineralogy, particle size distribution, surface irregularities, and structural anisotropy on strength dispersion.

In recent years, significant advancements have been made in understanding the mechanisms of particle breakage. Kuang et al. (2023) used heterogeneous discrete

element method (DEM) simulations to investigate how internal microstructures influence fracture initiation and strength, demonstrating that microstructural heterogeneity governs crack initiation sites and propagation paths. Zhang et al. (2024) provided a comprehensive review of DEM-based modeling approaches for particle crushing in geotechnical and mining contexts, recommending a hybrid modeling strategy that combines the bonded-particle model (BPM) with the fragment replacement method (FRM) to enhance simulation fidelity and computational efficiency. Additionally, Rotter et al. (2024) proposed a multiscale bonded-network reconstruction technique to improve the representation of brittle particle fragmentation within BPM frameworks. Recent studies have also highlighted the evolution of micromechanical parameters—such as force chains, contact density, and coordination number—in DEM simulations, offering critical insights into the link between microscale particle interactions and macroscale mechanical behavior.

For granular assemblies, existing research has shown that crushing behavior is governed not only by the intrinsic strength of individual particles, but also strongly influenced by factors such as particle gradation, initial packing density, confining pressure, stress path, and moisture conditions. For example, Gao et al. (2023) demonstrated through loess compression tests that the coupled effects of stress level and confining pressure significantly affect both the particle breakage ratio and dilatancy behavior, providing insight into the volumetric deformation induced by crushing. Similarly, Jia et al. (2022) systematically investigated the evolution of breakage modes in basalt rockfill under complex loading and wetting conditions, proposing a stress-path-dependent mechanism for particle failure in high-stress environments.

Despite these advances, the progressive breakage behavior of soft rock residuals—such as phyllite—under both continuously graded and single-sized conditions remains

insufficiently understood. In particular, the bidirectional coupling between particle breakage and gradation evolution, the patterns of breakage-induced deformation, and the influence of particle structural characteristics on macroscopic stress–strain behavior require further investigation through integrated physical testing and numerical simulation. These represent the central scientific questions addressed in this study.

In summary, to address the unclear role of gradation and the poorly understood coupling mechanisms between breakage and gradation evolution in soft rock residual fills, this study investigates the breakage characteristics of phyllite residuals generated during subgrade construction along Section S44 of the Kangluo Expressway. Recognizing that understanding single-particle crushing behavior is foundational to modeling aggregate breakage, we first conduct a series of single-particle compression tests to characterize breakage modes and establish strength–size relationships. These results are then used to calibrate key parameters in the development of DEM simulations. Subsequently, confined compression tests are conducted on phyllite specimens with different continuous and single-size gradations to examine their breakage behavior and stress–strain response under loading. This integrated approach aims to provide a robust experimental and numerical framework for predicting the mechanical performance and deformation behavior of soft rock residual fills while offering practical guidance for material utilization and engineering design in infrastructure projects.

2 Materials and Methods

2.1 Experimental Materials

The experimental material used in this study was phyllite residual waste produced during tunnel excavation along Section S44 of the Kangluo Expressway in Gansu Province, China. Phyllite is a low-grade metamorphic soft rock characterized by well-

developed joints and fissures, with significant heterogeneity in weathering degree even within individual samples. The material exhibits pronounced water sensitivity, low mechanical strength, and a high propensity for fragmentation under loading.

X-ray diffraction (XRD) analysis was conducted on the phyllite particles, and the results are presented in Fig. 1(a). The diffraction patterns indicate that the dominant mineral constituents include muscovite (38%), which exhibits pronounced basal cleavage, and kaolinite (22.5%), a clay mineral prone to hydration-induced softening. Orthoclase (27.1%) and quartz (12.4%) were also identified, with quartz and muscovite observed to cluster unevenly within the particle matrix. Muscovite and kaolinite are representative layered silicate minerals composed of SiO_4 tetrahedral sheets and Al–O octahedral sheets, weakly bonded by interlayer potassium ions. This structural arrangement results in excellent basal cleavage in muscovite, facilitating water penetration between the layers, weakening the interlayer K^+ bonds, and ultimately causing interlayer separation and sliding (Zhang et al., 2020). Consequently, the material is highly moisture-sensitive and prone to disintegration due to muscovite delamination and kaolinite swelling, both of which significantly reduce its mechanical strength. Moreover, the relatively high kaolinite content reflects active weathering, indicating a loosely bonded and inherently fragile rock structure. These mineralogical features collectively explain the engineering behavior of phyllite as a water-unstable, low-strength, and easily crushable soft metamorphic rock.

Scanning electron microscopy (SEM) images of the phyllite particles are shown in Fig. 1(b). The micrographs reveal a characteristic flaky–scaly morphology with rough surfaces and visible signs of interlayer exfoliation. This microstructure reflects the presence of densely distributed cleavage planes within the particles, which act as intrinsic mechanical weak zones. These planes significantly diminish the material's

shear and tensile strength, particularly along directions parallel to the foliation. Both external mechanical loading and internal pore water pressure can readily initiate failure along these pre-existing planes. The observed morphology corresponds to cleavage development commonly associated with layered silicate minerals such as muscovite and kaolinite.

Combined findings from the XRD and SEM analyses elucidate the fundamental causes of phyllite's poor engineering performance, notably its water sensitivity, strength degradation, and fragmentation tendency. These behaviors are intrinsically linked to the rock's mineralogical composition—rich in moisture-responsive layered silicates—and its foliated texture formed during metamorphism. The non-uniform spatial distribution of minerals further exacerbates internal heterogeneity and mechanical weakness. Upon water infiltration, mechanisms such as muscovite delamination, kaolinite swelling, and hydraulic wedging destabilize interparticle bonds, ultimately leading to disintegration and rapid strength loss. The elevated kaolinite content also signifies ongoing weathering processes that enlarge internal fissures and further weaken the structural integrity of the material. As a result, the phyllite residuals exhibit a high susceptibility to particle breakage under applied stress.

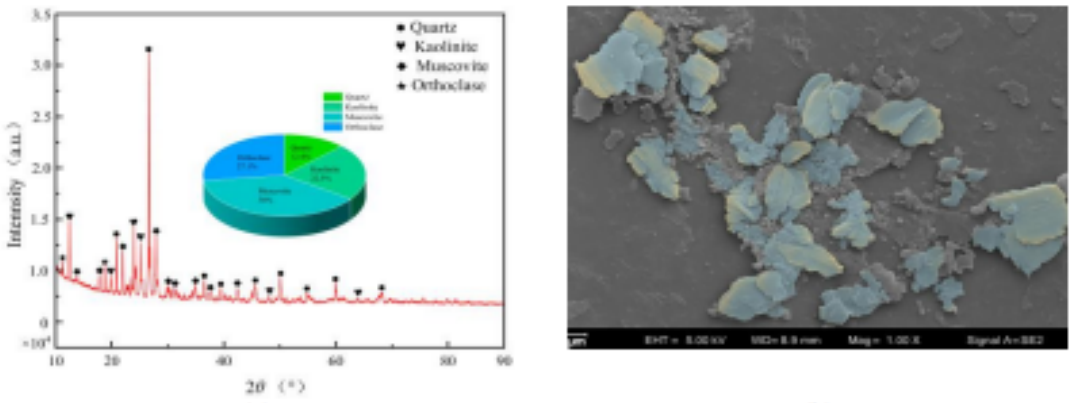

(a) (b)

Fig. 1 X-ray diffraction (XRD) pattern, mineral composition, and scanning electron microscopy (SEM) image of weathered phyllite residual particles.

The raw phyllite residual blocks collected from the construction site exhibited

substantial variability in size. Before testing, the materials were subjected to primary comminution using a jaw crusher to reduce all particle sizes to below 50 mm. The resulting crushed particles were subsequently sieved into five distinct size fractions: 5–10 mm, 10–16 mm, 16–20 mm, 20–25 mm, and 25–31.5 mm.

2.2 Experimental Equipment and Testing Procedure

The single-particle crushing tests were conducted using a Meters CDT1305-2 microcomputer-controlled electronic universal testing machine, as shown in Fig. 2(a). The apparatus features a maximum loading capacity of 300 kN, a force resolution of 0.01 kN, and a controllable displacement rate ranging from 0.01 to 50 mm/min. For all tests in this study, a constant loading rate of 2 mm/min was adopted. A total of 400 phyllite particles were randomly selected for testing, with 80 individual particles drawn from each of the five pre-sieved size fractions, as illustrated in Fig. 2(b).

The testing system comprises three primary components: a computer interface, a control and data acquisition unit, and a mechanical loading frame. Given the relatively large gap between the machine's loading platens, high-strength metal spacers were inserted to ensure stable and uniform contact with the test specimens. The compressive strength of the spacers was substantially higher than that of the weathered phyllite particles, thereby minimizing the risk of system-induced deformation and ensuring that the measured failure loads accurately reflected the intrinsic crushing strength of the particles.

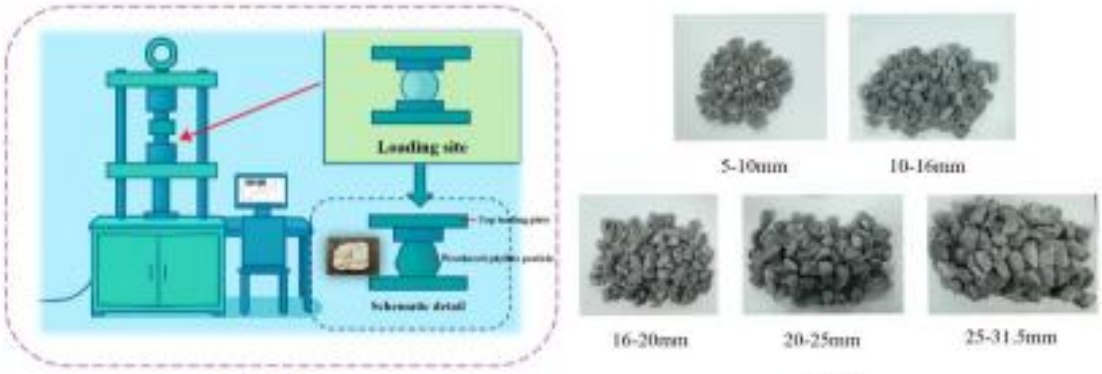

Fig. 2 Loading apparatus and phyllite particle specimens used for single-particle crushing tests.

During testing, each particle was repositioned multiple times to ensure a stable orientation between the loading platens that minimized initial stress concentrations. The lower platen was then gradually raised until contact with the upper platen was achieved, at which point the vertical gap between the platens was recorded as the initial loading height d (Wang et al., 2023). Loading was then initiated, and the test was terminated upon observation of a through-going crack or large-scale fragmentation in the phyllite particle, signifying structural failure. The corresponding failure load F_f was extracted from the load–displacement curve and used for subsequent calculation and analysis of the particle's crushing strength.

In engineering practice, phyllite residuals used as subgrade fill are subjected to compressive deformation under repeated traffic loads, leading to progressive particle breakage. This mechanical behavior can be effectively approximated by a confined compression model subjected solely to vertical loading (Xu et al., 2011). To evaluate the effect of particle gradation on the mechanical response of phyllite residuals, a series of confined compression tests was conducted under varying gradation conditions. The resulting stress–strain data were used to calibrate the discrete element method (DEM) model developed in this study.

The confined compression tests were performed using a YAW-4306 microcomputer-controlled electro-hydraulic servo testing machine, which offers a

maximum loading capacity of 3000 kN and a stroke length of 200 mm. The test setup incorporated a custom-fabricated steel confining cylinder with an internal diameter of 300 mm, a height of 300 mm, and a wall thickness of 16 mm, constructed from 20# low-carbon steel. Axial loading was applied at a constant displacement rate of 2 mm/min through a hydraulically driven closed-loop servo control system. Load and displacement signals were continuously monitored and recorded using high-precision sensors, with a measurement accuracy of ±1% for both parameters.

To reduce interface friction between the inner wall of the steel cylinder and the specimen—thereby facilitating specimen extraction post-loading—a thin, uniform layer of petroleum jelly was applied to the cylinder wall prior to testing.

Phyllite residuals used as subgrade fill materials exhibit pronounced sensitivity to gradation in their mechanical behavior. Previous studies have demonstrated that both particle size and gradation characteristics significantly influence the load-bearing performance of granular fills. Building upon these findings, this section presents a series of experimental investigations from two perspectives: single-sized gradation specimens and continuously graded specimens.

Two types of specimen configurations were prepared for testing. The single-sized gradation group (B1–B3) comprised particles in the size ranges of 5–10 mm, 10–20 mm, and 20–31.5 mm, respectively. The continuous gradation group (A1–A3) followed Talbot distributions with gradation indices n = 0.3, 0.5, and 0.7. A summary of the testing matrix is provided in Table 1.

Each continuously graded specimen, with a total mass of 33.5 kg, was prepared using a layered vibration compaction method, yielding an initial porosity of 0.384.

Given the uniformity in particle size, the single-sized specimens were compacted to a fixed height of 300 mm using the same method, resulting in specimen masses ranging from 25 to 30 kg and initial porosities between 0.448 and 0.540.

To capture the complete nonlinear response of the stress–strain relationship, the maximum axial stress was set at 15 MPa. This loading condition provides a full reference curve for the calibration of discrete element method (DEM) simulations across the entire loading cycle. All tests were conducted within a steel confining cylinder with an internal diameter of 300 mm, ensuring a diameter-to-maximum particle size ratio of approximately 9.5, thereby satisfying the size-effect criteria for compression testing of granular materials.

$$P_i = \left(\frac{d_i}{d_m}\right)^n \times 100\% \quad (1)$$

Where P_i is the passing percentage of particles at size (%); d_i is the particle size of each gradation level (mm); d_m is the maximum particle size of the continuously graded phyllite specimen (31.5 mm); n is the Talbot gradation index.

Table 1 Test matrix for confined compression tests

Test ID	5~10	10~16	16~20	20~25	25~31.5	10~20	20~31.5	Maximum Pressure (MPa)
A1	70.88	10.73	5.65	6.04	6.70	\	\	15
A2	56.34	14.93	8.41	9.41	10.91	\	\	15
A3	44.79	17.45	10.52	12.30	14.94	\	\	15
B1	100	\	\	\	\	0	0	15
B2	0	\	\	\	\	100	0	15
B3	0	\	\	\	\	0	100	15

3 Experimental Results

3.1 Analysis of Single-Particle Crushing Strength and Size Effect

The strength of granular materials is one of their most fundamental mechanical properties and serves as a key parameter distinguishing them from continuum materials. Understanding the statistical distribution of particle strength holds considerable practical significance for a wide range of engineering applications. In single-particle compression tests, crushing strength is typically characterized by the particle's crushing stress. Based on the formulation proposed by Jaeger (1967), the crushing strength of an individual particle can be determined using Equation (2):

$$\sigma_f = \frac{F_f}{d_0^2} \tag{2}$$

where σ_f is the crushing stress of the particle, F_f is the peak load at the point of particle failure (obtained from the load–displacement curve), and d_0 is the effective loading length, i.e., the initial vertical height of the particle when it just contacts both loading plates.

Due to the presence of numerous internal fissures, pores, and structural defects, phyllite particles exhibit significant heterogeneity in their mechanical properties. Additionally, variations in weathering degree—arising from differences in stratigraphic and environmental conditions, even within the same excavation site—further contribute to the pronounced dispersion in single-particle strength (Lobo-Guerrero and Vallejo, 2006). As a brittle material characterized by inherently high strength variability, phyllite is well suited to statistical modeling approaches.

Previous studies have shown that the Weibull distribution function (Weibull, 1951)

provides a reliable framework for describing the strength distribution of such heterogeneous materials. Its applicability has been extensively validated across a wide range of geotechnical granular materials (Zhang et al., 2016). Accordingly, the present study adopts the Weibull distribution to analyze the probabilistic behavior of strength variation in phyllite particles.

Single-particle crushing tests were performed on a series of phyllite specimens, and the test results were subjected to statistical analysis. The survival probability of particles, denoted as P_s, was calculated using Equation (3):

$$P_s = \frac{N(\sigma \leqslant \sigma_f)}{N} \tag{3}$$

where N is the total number of tested particles; N（$\sigma \leq \sigma_f$）is the number of particles in the group that remained unbroken under the applied stress σ.

The breakage of phyllite particles is treated as a probabilistic event, wherein the survival probability P_s is assumed to follow a Weibull distribution as a function of the applied stress, as expressed in Equation (4):

$$p_s = \exp\left[-\left(\frac{\sigma_f}{\sigma_0}\right)^m\right] \tag{4}$$

where σ_0 is the characteristic strength of the particles corresponding to a survival probability P_s=37% (MPa); the particle size corresponding to σ_0 is referred to as the characteristic particle size d_0 (mm); m is the Weibull modulus.

Taking the natural logarithm of both sides of Equation (3.3) yields the linearized form shown in Equation (5):

$$\ln\left[\ln\left(\frac{1}{P_s}\right)\right] = m\ln(\sigma_f) - m\ln(\sigma_0) \tag{5}$$

$\ln(\sigma_f)$ coordinate system and fitted using linear regression. As shown in Fig. 3, the Weibull distribution fit for the 5–10 mm phyllite size group is presented; results for the other size groups are provided in the table. In this plot, the slope of the fitted line corresponds to the Weibull modulus m, while the intercept represents $m\ln(\sigma_0)$ is the characteristic strength.

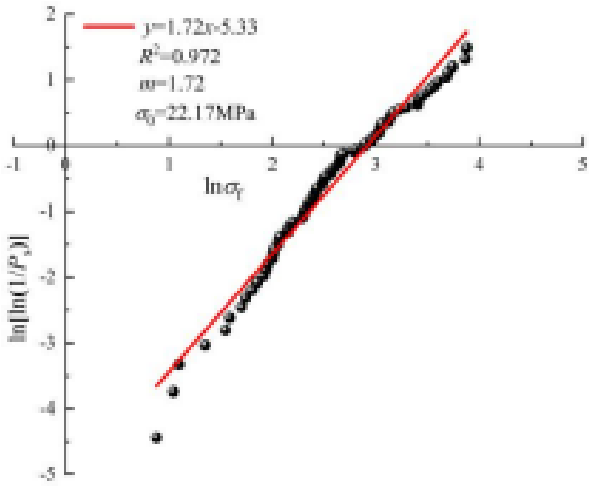

Fig. 3 Crushing strength–survival probability relationship for 5–10 mm phyllite particles

The crushing strength of phyllite particles conforms to the Weibull distribution, as shown in Fig. 3. The Weibull modulus m obtained for the five particle size groups in this study was 1.72 (5–10 mm), 1.70 (10–16 mm), 1.59 (16–20 mm), 1.51 (20–25 mm), and 1.25 (25–31.5 mm), respectively. The value of m exhibits a clear decreasing trend with increasing particle size, ranging from 1.25 to 1.75 overall.

As an intrinsic material parameter, the Weibull modulus m quantifies the degree of strength variability: higher m values correspond to lower strength dispersion and indicate greater material homogeneity (Meng et al., 2022). The observed decrease in m with increasing particle size—amounting to a total reduction of 28.57%—suggests that

strength variability becomes more pronounced as particle size increases (Cai et al., 2025). Detailed Weibull fitting parameters for each particle size group are provided in Table 2.

Based on the results of single-particle crushing tests, this study systematically investigated the relationship between particle crushing strength σ_f and characteristic strength σ_0 across different particle size groups. As illustrated in Fig. 4, the crushing strength σ_f of phyllite particles exhibits a clear decreasing trend with increasing effective loading height d, which serves as a proxy for particle size.

Table 2 Weibull fitting parameters for phyllite particles of different size groups

Particle Size Group d (mm)	Average Loading Height d_{avg}(mm)	Weibull Modulus m	Characteristic Strength σ_0(MPa)	Characteristic Size d_0(mm)
5~10	6.74	1.72	22.17	7.55
10~16	10.87	1.70	20.20	10.70
16~20	13.57	1.59	19.10	18.31
20~25	17.58	1.51	13.59	21.21
25~31.5	20.00	1.25	11.38	25.50

The average crushing strengths for the five particle size groups, ordered from smallest to largest, were 16.58 MPa, 14.41 MPa, 12.81 MPa, 10.52 MPa, and 9.82 MPa, respectively. This represents an overall reduction of 6.76 MPa, corresponding to a relative decrease of 40.77%.

This trend clearly demonstrates a pronounced size effect in both the particle crushing strength σ_f and the characteristic strength σ_0. Under the same level of applied stress, larger phyllite particles are more prone to breakage compared to smaller ones. This can be attributed to the fact that larger particles typically contain more internal and surface flaws—such as cracks, pores, and structural defects—which act as stress

more likely to initiate at these weak points in larger particles under compressive loading.

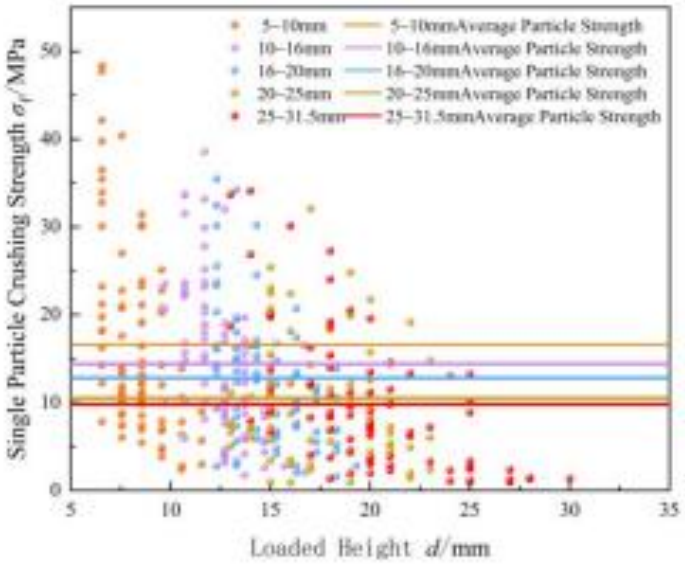

Fig. 4 Relationship between single particle crushing strength and particle size for phyllite residuals.

3.2 Stress–Strain Relationships of Phyllite Residuals with Different Gradations

Based on the experimental protocol outlined in Section 2.2, confined compression tests were performed on the specimen groups listed in Table 1 using an electro-hydraulic servo-controlled loading system. Axial load and displacement were continuously recorded in real time throughout the loading process. Given that the stiffness of the confining apparatus was substantially greater than that of the phyllite residual specimens, lateral deformation was considered negligible. Accordingly, the deformation behavior was simplified to a uniaxial compression model.

The axial strain ε_v was calculated using Equation (6), defined as the ratio of axial displacement to the initial specimen height (300 mm). The axial stress σ_v was determined using Equation (7), defined as the applied axial load divided by the cross-sectional area of the loading plate.

$$\varepsilon_v = \frac{\Delta h}{h} \tag{6}$$

where Δh is the axial displacement of the phyllite residual specimen (mm); h is the initial height of the specimen, which is 300 mm.

$$\sigma_v = \frac{F}{\pi R^2} \tag{7}$$

where F is the axial force applied to the phyllite residual specimen during loading (N); R is the radius of the loading plate, which is 150 mm.

After the completion of the tests, the monitored data were used to calculate the stress–strain responses of the specimens. The stress–strain curves for the continuously graded specimens are shown in Fig. 5(a), while those for the single-sized graded specimens are presented in Fig. 5(b).

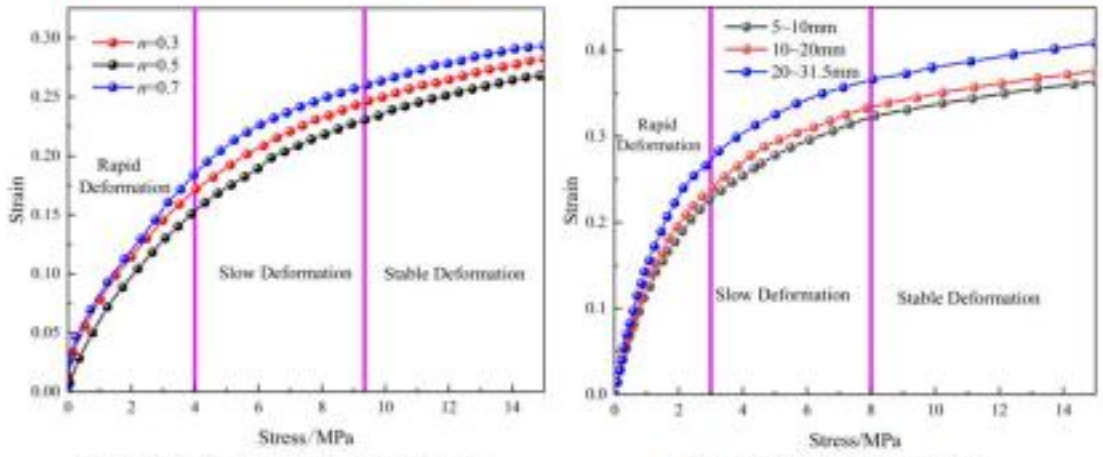

（a）continuously graded specimens　　（b）single-sized specimens

Fig. 5 Stress–strain curves of phyllite residual specimens under confined compression.

As shown in Fig. 5, with increasing vertical stress, the axial strain of both continuously graded and single-sized phyllite specimens increases correspondingly, while the growth rate of the stress–strain curves gradually declines. The overall deformation process can be divided into three distinct stages: rapid deformation, slow deformation, and stable deformation.

In the rapid deformation stage, porosity decreases sharply as the initially loose granular structure compacts rapidly, resulting in a steep increase in axial strain. During the subsequent slow deformation stage, secondary structural adjustments occur through frictional sliding and the breakage of larger particles within the now denser granular skeleton. In the final stable deformation stage, remaining voids are progressively compressed, and fine particles generated from breakage fill intergranular spaces, leading to a more continuous and homogenized particle framework. At this stage, smaller particles become more resistant to further breakage, and the rate of axial strain increment significantly decreases. This staged evolution reflects a mechanical transition of phyllite residuals from a discrete particulate system to a quasi-continuous medium, governed sequentially by particle rearrangement, friction–breakage interactions, and cooperative load-bearing between coarse and fine particles.

As depicted in Fig. 5(a), under an axial stress of 15 MPa, specimen A2 (Talbot index n=0.5) from the continuously graded group exhibited the lowest axial strain (0.27), which is 6.9% lower than that of specimen A3, the most deformable among the continuously graded samples. In contrast, the minimum axial strain observed among the single-sized specimens was 0.36 (specimen B1), representing a 33.3% increase compared to A2.

This result is consistent with the findings of Cao and Wang (2005). They reported that a Talbot gradation with an index of n=0.5 yields an optimized load-bearing structure. This is achieved by maximizing the coordination between coarse and fine

particles, thereby minimizing deformation under identical loading conditions.

Overall, under the same axial stress level, the axial deformation resistance of continuously graded specimens was superior to that of single-sized specimens. From the perspective of strain control, phyllite residuals with a Talbot gradation index of n =0.5 (specimen A2) are considered the most suitable for use as subgrade fill materials.

3.3 Analysis of Breakage Characteristics of Phyllite Residuals with Different Gradations

3.3.1 Particle Size Distribution Analysis Before and After Testing

A particle size distribution analysis was conducted on the continuously graded specimens to evaluate their breakage behavior. The mass proportion changes in each particle size group before and after the confined compression tests were plotted, as shown in Fig. 6. Post-test results revealed a significant reduction in the mass proportion within the 5–31.5 mm size range. Specifically, the fine particle group (5–10 mm) exhibited a reduction in mass proportion ranging from 25.19% to 30.13%, while the coarse particle groups (10–31.5 mm) experienced more substantial losses, with reductions ranging from 34.20% to 44.29%. The decline in mass proportion was clearly more pronounced in the larger particle groups compared to the smaller ones. Moreover, within each specimen, the extent of mass loss increased consistently with particle size.

This trend can be attributed to two primary factors. First, phyllite residuals display a strong particle size effect, wherein larger particles have a higher intrinsic probability of breakage due to structural heterogeneity. Second, larger particles are subjected to more contact points and tend to experience higher local contact stresses, thereby

particles undergo more severe crushing, leading to a greater reduction in their post-test mass proportion.

The Talbot gradation index *n* exerts a notable regulatory influence on the breakage characteristics of the specimens. For the fine particle group (5–10 mm), the reduction in mass proportion was 30.13%, 28.99%, and 25.19% for specimens A1 (n=0.3), A2 (n=0.5), and A3 (n=0.7), respectively—showing a decreasing trend with increasing Talbot index. In contrast, the coarse particle groups (10–31.5 mm) exhibited mass losses of 38.32%–41.78% for A1, 34.20%–42.08% for A2, and 42.31%–44.29% for A3, demonstrating a clear increasing trend as *n* increased.

This behavior is primarily attributed to differences in the initial gradation structure. Specimen A1, dominated by fine particles (with the 5–10 mm fraction accounting for over 70% of the total mass), forms a densely packed structure in which the primary load-transfer paths are established between fine particles. Consequently, the fine fraction in A1 experiences the most severe mass loss due to crushing. In contrast, specimen A3 exhibits a relatively loose packing structure dominated by coarse particles (with the 10–31.5 mm fraction making up over 55% of the mass), which concentrates stress within the coarse particle framework and leads to more extensive breakage in the larger size fractions. Specimen A2 represents a well-graded, compact structure in which both fine and coarse particles contribute meaningfully to the load-bearing skeleton. This facilitates a more uniform distribution of contact stress, resulting in intermediate levels

of breakage for both fine and coarse particle groups.

These results demonstrate that the Talbot gradation index n plays a critical role in governing the evolution of particle breakage by modulating the internal force transmission network within granular assemblies.

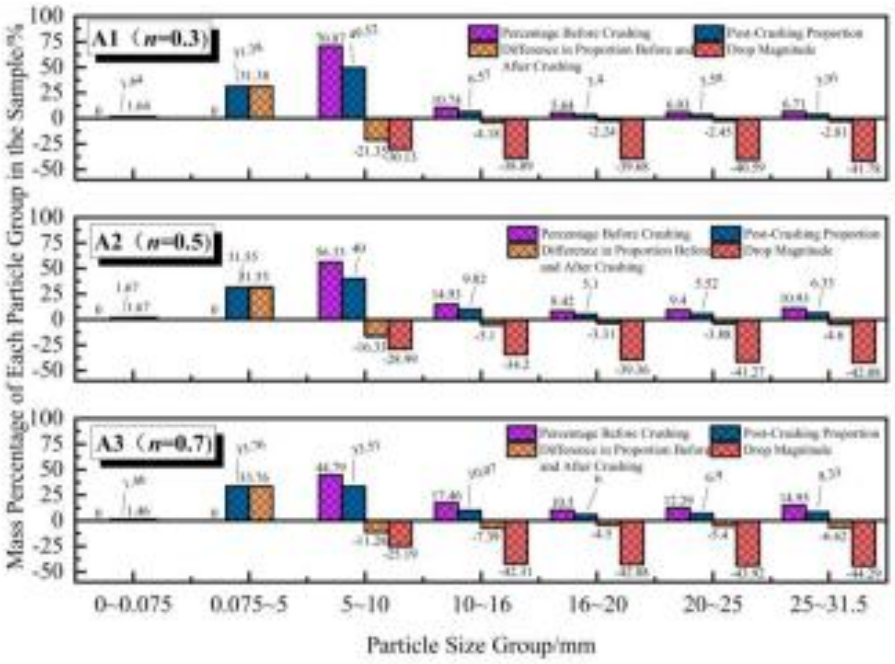

Fig. 6 Particle size distributions of continuously graded specimens A1–A3 before and after confined compression.

3.3.2 Analysis of Particle Breakage Ratio in Phyllite Residual Specimens

Numerous scholars, both domestically and internationally have investigated the phenomenon of particle breakage. Studies have shown that particle breakage significantly alters the original gradation curve of granular materials, and that comparing particle size distributions before and after testing provides a direct and accurate means of quantifying the degree of breakage. Hardin (1985) introduced the concept of breakage potential into the study of granular materials and defined key parameters including the amount of breakage (B_t), residual breakage potential, and total

breakage potential（B_p）. The total breakage potential is defined as the sum of the amount of breakage and the residual breakage potential and is determined by the minimum particle size present in the specimen. In Hardin's analysis, particles with diameters less than or equal to 0.074 mm are considered incapable of further breakage, and this size is therefore adopted as the lower limit for breakage potential calculations (Fig 7).

In this study, Hardin's relative breakage model is used to quantify the extent of particle breakage in the phyllite residual specimens. The calculation formula is presented in Equation (8):

$$B_r = \frac{B_t}{B_p} \tag{8}$$

where B_r is the relative breakage ratio of the specimen (%); B_t is the amount of breakage; B_p is the total breakage potential.

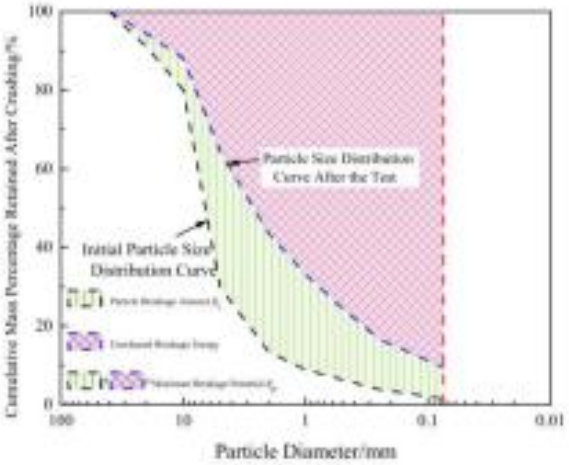

Fig. 7 Illustration of Hardin's relative breakage ratio model.

Sieve analysis was conducted on each specimen before and after the confined compression tests to determine the mass distribution across different particle size groups. The gradation curves were plotted using a semi-logarithmic coordinate system,

where the logarithm of sieve aperture size was used as the horizontal axis and the retained mass fraction as the vertical axis. Both continuously graded and single-sized specimens were analyzed in this manner. The relative breakage ratio B_r for each specimen was calculated using the built-in integration function in Origin software, based on Hardin's model.

The calculation results are shown in Table.3, where subfigures (a–c) present the relative breakage ratios of the continuously graded specimens, and subfigures (d–f) correspond to the single-sized specimens.

Table 3 Relative Breakage Ratio for Different Gradation Conditions

Gradation Type	ID	Gradation Parameters	Relative Breakage Ratio Br / %
Continuous Gradation	A1	n=0.3	28.37
Continuous Gradation	A2	n=0.5	30.01
Continuous Gradation	A3	n=0.7	33.62
Single Particle Group	B1	5-10mm	36.01
Single Particle Group	B2	10-20mm	42.55
Single Particle Group	B3	20-31.5mm	46.84

The relative breakage ratio (B_r) of the phyllite residual specimens is significantly influenced by both the gradation type and particle size distribution. Among the continuously graded specimens, specimen A3 (n=0.7) exhibited the highest B_r value at 33.62%, followed by A2 (n=0.5) and A1 (n=0.3, 28.37%), indicating a clear positive correlation between the relative breakage ratio and the Talbot index n. Within the single-sized groups, specimen B3 (20–31.5 mm) showed the highest breakage ratio at 46.84%, followed by B2 (10–20 mm, 40.22%) and B1 (5–10 mm, 36.01%), demonstrating a strong positive relationship between breakage ratio and particle size.

This trend is primarily attributed to differences in the initial gradation structures.

For continuously graded specimens, an increase in the Talbot index n corresponds to a higher proportion of coarse particles (>10 mm), increasing from 44.79% in A1 to 55.21% in A3. Due to the size effect of particle strength, the inverse relationship between particle size and crushing resistance, the prevalence of larger particles leads to increased breakage. A similar mechanism is observed in the single-sized specimens, where the increase in B_r with particle size is directly governed by the negative correlation between particle diameter and strength.

Under an axial stress of 15 MPa, the relative breakage ratios for the continuously graded specimens (ranging from 28.37% to 33.62%) were significantly lower than those of the single-sized specimens (36.01%–46.84%). Likewise, the axial strain values of the continuously graded group (0.268–0.293) were markedly lower than those observed in the single-sized group (0.364–0.409), indicating superior overall engineering performance for the continuously graded phyllite residuals.

Considering both deformation resistance and breakage resistance, the continuously graded specimen with a Talbot index of n =0.5 (specimen A2) appears to offer the most favorable characteristics for subgrade fill applications. Under the same axial stress of 15 MPa, A2 exhibited an axial strain 5.2% lower than that of A1, while its relative breakage ratio was only 1.78% higher, demonstrating an optimal balance between structural stability and crushing resistance.

3.4 Discrete Element Modeling (DEM)

To investigate the mechanical behavior of phyllite residuals and comparable

rockfill materials, a numerical simulation framework based on the discrete element method (DEM) was developed in this study. As conventional continuum mechanics approaches are inadequate for capturing discrete phenomena such as particle rearrangement and breakage, the PFC3D platform was employed to construct a particle-based numerical model. This software utilizes particle discretization to simulate the evolution of contact force chains and particle crushing in granular geomaterials, thereby overcoming the inherent limitations of physical experiments in revealing micromechanical mechanisms.

The present simulation focuses on the crushing behavior of phyllite residuals under confined compression conditions, with the aim of systematically analyzing the relationship between breakage evolution and macroscopic mechanical response. The findings are intended to provide theoretical support for practical engineering applications.

Given the complexity of geotechnical systems, several assumptions were adopted in the modeling process: (1) particles are treated as rigid bodies; (2) inter-particle contacts are modeled as point contacts with assignable normal and tangential strength parameters; and (3) a soft contact model is used, allowing for particle "overlap" at contact points to represent local deformation and force transmission. Since individual particles in PFC3D are idealized as rigid spheres and lack deformability, clumps (or clusters) of bonded spheres were employed to approximate the morphology of irregularly shaped blocks, thereby compensating for the limitations associated with

spherical particle representation.

3.4.1 Contact Types and Contact Constitutive Models

In PFC simulations, two primary types of contact interactions are considered: ball–ball and ball–facet contacts. Contact forces are applied at the point of "overlap" between the interacting entities, as governed by the soft contact model.

For ball–ball contacts, the normal direction is defined by the line connecting the centers of the two contacting spheres. In the case of ball–facet contacts, the normal vector is determined by the shortest path from the center of the spherical particle to the plane representing the facet (i.e., wall surface). These contact geometries and force transmission directions are schematically illustrated in Fig. 8.

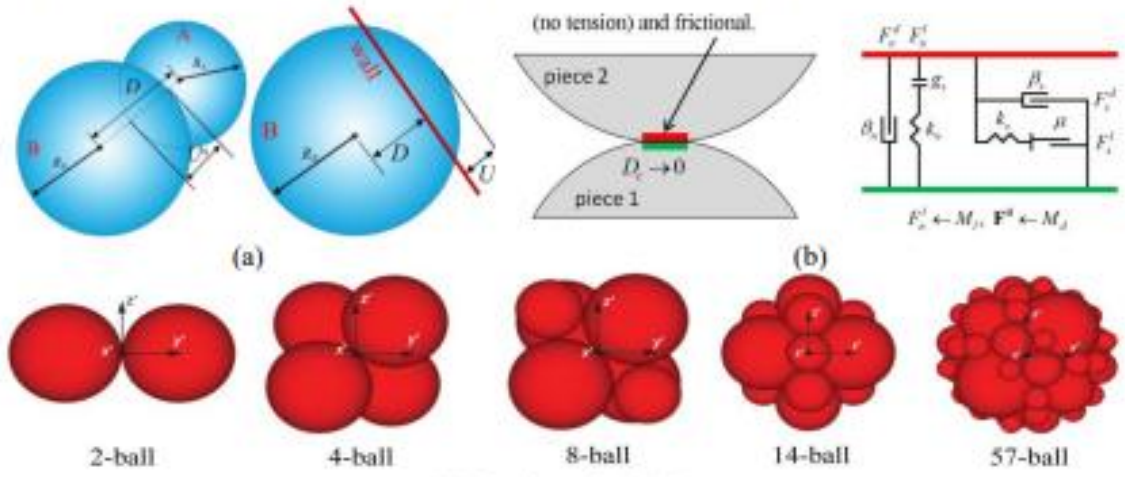

(c) Ciantia et al. (2015)

Fig.8 Two basic types of contact in PFC and mechanical response system of the linear contact model.

In PFC3D, the mechanical response system between particles is constructed by defining contact constitutive models such as stiffness models, slip models, and bonding models. In this study, the linear contact model is adopted as the constitutive relationship for both *ball–ball* and *ball–facet* contacts. This model incorporates constant normal and

shear stiffness parameters k_n、ks as well as a friction coefficient (μ), making it particularly suitable for representing the rough surface and highly crushable nature of phyllite residual particles (Zhang et al., 2017; Xu et al., 2024). As illustrated in Fig. 8, the mechanical mechanism of the model is represented by linear springs in both normal and tangential directions. The normal and shear stiffnesses are predefined and remain constant throughout the simulation. In the normal direction, a contact gap g_s is defined between interacting particles. The contact is activated only when $g_s \leq 0$, indicating particle overlap. In the tangential direction, a friction coefficient μ is applied to constrain the tangential force, which is computed as the product of μ and the corresponding normal force.

This model involves three key microscopic parameters: the effective modulus (E^*, *emod*), the stiffness ratio (k^*, *kratio*), and the friction coefficient (μ^*, *fric*). Among them, k^* represents the ratio of orthogonal stiffnesses, i.e., the ratio between the normal stiffness k_n and the shear stiffness k_s. This relationship is defined in Equation (9), where k_n primarily governs the linear force in the normal direction, while k_s governs the linear force in the tangential direction.

$$\kappa^* = \frac{k_n}{k_s} \tag{9}$$

The relationship between the effective modulus E^* and the normal stiffness k_n is given in Equation (10):

$$k_n = \frac{AE^*}{L} \tag{10}$$

In the equation: A is the contact area, with its calculation provided in Equations (9)

and (10); L is the center-to-center distance for *ball-ball* contacts, or the perpendicular distance from the ball center to the wall for *ball-facet* contacts, as defined in Equation (11):

$$A = \begin{cases} 2rt, 2\mathrm{D}(t=1) \\ \pi r^2, 3\mathrm{D} \end{cases} \tag{11}$$

$$r = \begin{cases} min\left(R^{(1)}, R^{(2)}\right), \mathrm{ball-ball} \\ R^{(1)}, \mathrm{ball-facet} \end{cases} \tag{12}$$

$$L = \begin{cases} R^{(1)} + R^{(2)}, \mathrm{ball-ball} \\ R^{(1)}, \mathrm{ball-facet.} \end{cases} \tag{13}$$

Figure 8 Illustration of r, $R^{(1)}$, and $R^{(2)}$ in Equations (11–13)

3.4.2 Breakage Modeling Methods and Breakage Criteria

Within the framework of the discrete element method (DEM), particle breakage is primarily modeled using two approaches: the Bonded-Particle Method (BPM) and the Fragment Replacement Method (FRM). In BPM, each particle is represented as an agglomerate of multiple bonded rigid sub-particles, allowing for a more realistic approximation of actual particle geometry and internal structure. This method is particularly effective for simulating breakage behavior in single particles or small-scale particle assemblies (Tapias et al., 2012). However, BPM is computationally intensive and does not support secondary fragmentation of sub-particles, which limits its applicability in capturing the progressive breakage commonly observed in soft rock materials.

In contrast, FRM does not replicate the exact morphology of natural particles but

offers significantly higher computational efficiency. Upon meeting a predefined breakage criterion, a parent particle is replaced by a set of smaller, preconfigured sub-particles. This approach is especially suitable for large-scale simulations, as it allows for recursive fragmentation and better reflects the staged crushing process of soft rock aggregates. Given the substantial and continuous breakage observed in phyllite residuals under confined compression, FRM was adopted in this study to balance computational efficiency with adequate physical fidelity in modeling the complete breakage evolution.

Two key parameters govern FRM implementation: the number of sub-particles and the breakage criterion. The number of sub-particles affects both the computational cost and the resolution of fragmentation, while the breakage criterion determines the physical plausibility of breakage initiation. Due to the inherent variability in particle geometry and material defects, experimental observations of fragment counts often exhibit large fluctuations. Therefore, the selection of these modeling parameters must be optimized based on material characteristics and empirical evidence to enhance the robustness and accuracy of simulation outcomes.

With respect to sub-particle configurations, Ciantia et al. (2015) proposed five Apollonian-based replacement schemes involving 2, 4, 8, 14, and 57 sub-particles. These schemes have been successfully applied in confined compression simulations to reflect different levels of fragmentation, as illustrated in Fig. 8(c).

Research findings have shown that both the 14-sub-particle and 57-sub-particle

Apollonian replacement schemes are capable of accurately reproducing the results of laboratory-scale particle breakage tests. However, the 14-sub-particle configuration offers a significant advantage in terms of computational efficiency while maintaining a high degree of accuracy. Therefore, in this study, the 14-particle Apollonian packing scheme is adopted as the preferred fragment replacement strategy for implementing the Fragment Replacement Method (FRM) in the DEM-based simulation of particle breakage.

Regarding the selection of breakage criteria, there is currently no universally accepted standard for DEM simulations of particle fragmentation. Most existing criteria are extensions of the stress-based and force-based thresholds originally proposed by Åström and Herrmann (1998). These criteria typically define a critical force or stress level, beyond which a particle is assumed to fail and disintegrate. However, within granular assemblies, the stress state of individual particles is influenced by complex inter-particle interactions and multi-directional loading paths. As a result, the actual breakage strength of a particle embedded within an assembly may exceed that observed in isolated single-particle tests. This discrepancy implies that simplified metrics such as average or maximum contact force or stress may not reliably capture the onset of breakage in realistic particulate systems.

To address this limitation, McDowell and De Bono (2013) proposed the use of the octahedral shear stress criterion, which incorporates the characteristic strength σ_0 obtained from single-particle crushing tests as the critical stress threshold for breakage

initiation. This criterion accounts for the three-dimensional stress state experienced by particles within an assembly and has demonstrated improved predictive capability. The mathematical formulation of this criterion is provided in Equation (14):

$$q = \frac{1}{3}[(\sigma_1 - \sigma_2)^2 + (\sigma_2 - \sigma_3)^2 + (\sigma_3 - \sigma_1)^2]^{\frac{1}{2}} \quad (14)$$

where σ_1, σ_2, and σ_3 represent the first, second, and third principal stresses of the particle, respectively.The stress tensor σ_{ij} for each particle in the discrete element method is calculated using Equation (15):

$$\sigma_{ij} = \frac{1}{V}\sum_{n_c} f_j^c d_i^c \quad (15)$$

where V denotes the volume of the particle, η_c is the total number of contact forces acting on the particle, η_c represents the contact force at contact c, and d_i^c is the branch vector from the particle center to the contact point. The principal stresses σ_1、σ_2、σ_3 correspond to the normal stress components σ_{11}、σ_{22}、σ_{33}, respectively.

De Bono and McDowell (2014) proposed that the octahedral shear stress-based breakage criterion can be characterized by a critical stress threshold, denoted as $[q]$, which represents the particle's allowable stress limit. The value of [q] is calculated using Equation(16).During the discrete element simulation, a particle is considered to undergo breakage when its octahedral shear stress, calculated via Equation (16), reaches or exceeds the threshold (i.e., $q \geq [q]$).

$$[q] = 0.9\sigma_f = \frac{0.9F_f}{d^2} \quad (16)$$

Where σ_f denotes the crushing strength of the particle.

Phyllite rock waste is a naturally brittle material, and its particle crushing strength

exhibits a Weibull distribution.

Moreover, based on Weibull statistical theory and the concept of size effect (Bažant, 1984), the crushing strength σ_f of an individual particle can be calculated using Equation (17).In this equation, the term $(d/d_0)m^{-3/m}$ is introduced to account for the size effect of phyllite particles, where d is the particle diameter, d_0 is a reference diameter, and m is the Weibull modulus.

$$\sigma_f = \left[\ln\left(\frac{1}{P_s(d)}\right)\right]^{\frac{1}{m}} \left(\frac{d}{d_0}\right)^{-\left(\frac{3}{m}\right)} \sigma_0 \tag{17}$$

Where P_s (d) denotes the survival probability of a particle of size d, which is modeled in the discrete element simulation as a random number uniformly distributed between 0 and 1.

Accordingly, during DEM simulations, a particle is considered to break when the applied stress satisfies Equation (18):

$$q \geqslant [q] = 0.9\left[\ln\left(\frac{1}{P_s(d)}\right)\right]^{\frac{1}{m}} \left(\frac{d}{d_0}\right)^{-\left(\frac{3}{m}\right)} \sigma_0 \tag{18}$$

3.4.3 Model Construction

The construction of the PFC3D numerical model involves five main steps: wall generation, particle generation, assignment of contact parameters, loading application, and data monitoring/post-processing. The final numerical specimen configuration is shown in Fig. 9

A cylindrical wall is used to replicate the confining steel barrel employed in the laboratory experiments, with a diameter of 300 mm to ensure consistency between the

numerical and physical setups. Rectangular walls are defined to represent the bottom cap and the axial loading platen. The gradation curves, particle size distributions, and porosities of the generated granular assemblies are matched to those of the laboratory-prepared specimens A1, A2, and A3. Accordingly, the corresponding numerical models are designated as A1-1, A2-2, and A3-3, respectively.

Following model initialization, loading is applied to simulate the confined compression process and capture particle breakage behavior. The loading rate is set to 2 mm/min, consistent with the laboratory conditions. A minimum breakage limit of 0.074 mm is imposed in the simulation, below which sub-particles are no longer allowed to undergo further fragmentation. This constraint helps prevent excessive computational cost while maintaining the physical relevance of the modeled breakage process. A1-1/A3-3 can be found in Figures S11/S12 in the Supplemental Materials section.

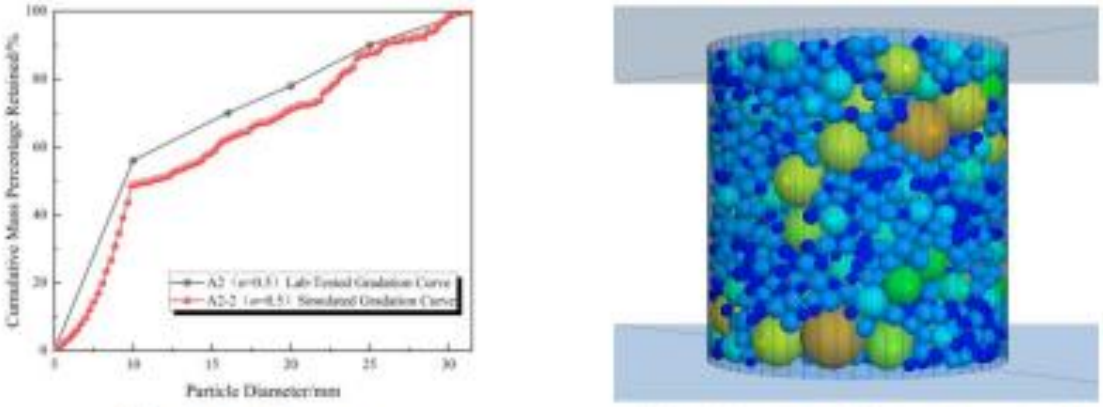

(a) A2-2 grading curve (b) A2-2 DEM model(Total Spheres: 3434)

Fig. 9 Numerical Model of Phyllite Residual Fill in Unconfined Compression Test with n=0.5

3.4.4 Parameter Calibration and Model Validation

A key challenge in simulating particle behavior using the discrete element method (DEM) lies in the selecting appropriate micromechanical parameters. Parameter calibration must balance physical realism with computational feasibility. Although several parameter calibration approaches have been applied to specific models, their general applicability remains limited due to differences in model structure and material properties. Currently, the mainstream calibration strategy still relies on a trial-and-error method based on sensitivity analysis. This process begins by identifying reasonable parameter ranges through sensitivity studies—e.g., normal stiffness k_n=0.5×10^7~1.0×10^7, stiffness ratio kratio=0.95~1.05, and inter-particle friction coefficient fric=0.4~0.7. These parameters are then systematically adjusted to fit the laboratory test results, typically aiming for an error margin of less than 10%. After extensive optimization, a set of micromechanical parameters suitable for simulating the confined compression and breakage behavior of phyllite rock waste was determined, as summarized in Table 4. The numerical simulation results obtained using these parameters were then compared with laboratory test results from specimens A1, A2, and A3. The comparison outcomes are shown in Fig. 10.

Table 4 Micromechanical parameter values

Model Entity	Micromechanical Parameter	Unit	Value
Particle Unit	Particle density（ρs）	kg/m3	2.564×103
	porosity	—	0.384
	Normal stiffness kn	N/m	0.49×107
	kratio	—	1
	fric	—	0.45
wall	Normal stiffness（kn）	N/m	0.49×108
	kratio	—	1

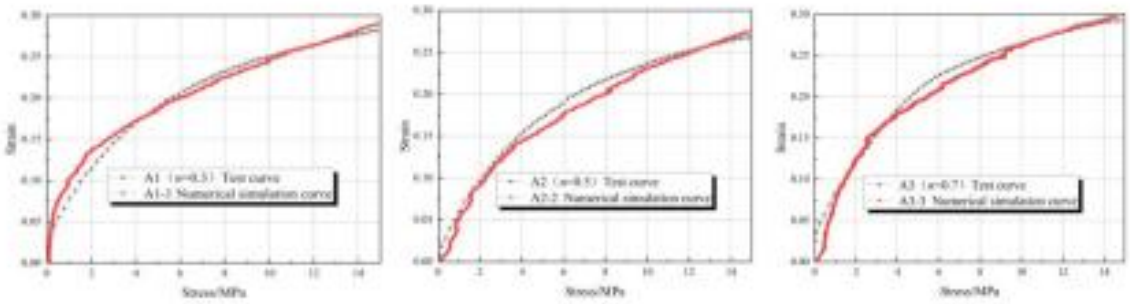

(a) A1 and A1-1 (b) A2 and A2-2 (c) A3 and A3-3

Fig. 10 Micromechanical parameter calibration and inversion curve

As shown in Fig. 10, the stress–strain curve obtained from the numerical model under loading agrees well with that from the laboratory test. Therefore, it is reasonable to use the micromechanical parameters listed in Table 4 for the numerical modeling of confined compression tests on phyllite rockfill, indicating that the parameter calibration is successful.

3.4.5 Analysis of the Dynamic Evolution Law of Particle Breakage Quantity

The micromechanical response mechanisms of phyllite rockfill during confined compression are investigated using numerical models. For clarity and consistency, the specimen identifiers remain consistent with those in Chapter 2. Specifically, the numerical models corresponding to the laboratory specimens with Talbot indices of n = 0.3 (A1), n = 0.5 (A2), and n = 0.7 (A3) are labeled as A1-1, A2-2, and A3-3, respectively.

During the numerical simulations, particles are categorized into two groups: parent particles that remain unbroken (group name: “None”) and newly generated fragments resulting from breakage (group name: “Break”). All broken fragments are visually distinguished by coloring them red. A FISH script is implemented to incrementally save

the simulation state at every 5% axial strain interval, continuing up to a final axial strain of 30%.

For visualization purposes, all results are presented from a unified front view, and the *wall* (representing the confining steel cylinder) is set to 70% transparency to enhance the visibility of particle breakage morphology.

To quantitatively assess the degree of particle breakage, the numbers of parent and fragment particles at various strain levels are extracted and statistically analyzed using FISH. The cumulative number of generated fragments under different axial strains is summarized in Table 5 The cumulative number of broken parent particles as a function of axial strain and Talbot index *n* is shown in Fig. 11.

Table 5 Cumulative number of fragment particles generated under different grading conditions with increasing axial strain

Strain（%）	0	5	10	15	20	25	30
A1-1	0	210	517	1145	1977	3261	5316
A2-2	0	867	1595	2485	3709	5136	7452
A3-3	0	560	882	1442	2109	3043	4283

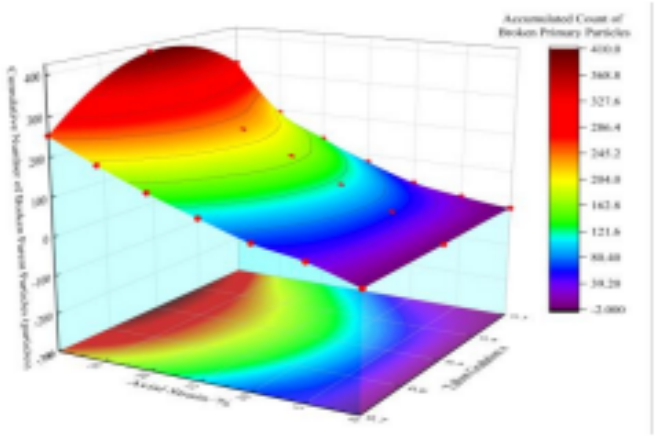

Fig. 11 Surface plot of the cumulative number of parent particle breakages with axial strain and talbot grading index *n*

As shown in Fig. 11, with increasing axial strain, all three numerical specimens (A1-1, A2-2, and A3-3) exhibit a synchronized growth trend in both the number of parent particle breakages and the generation of child particles. Moreover, the progression of breakage clearly demonstrated a strong dependency on the Talbot gradation index. At the terminal axial strain of 30%, quantitative results show that the cumulative number of child particles generated follows the order: A2-2 (7,452) > A1-1 (5,316) > A3-3 (4,283), with corresponding parent particle breakage counts of 406, 324, and 253, respectively. These yield child-to-parent particle number ratios in the range of 16.41 to 18.36.

It is noteworthy that the observed ratios (16.41, 18.36, 16.93) are significantly higher than the single-step substitution value of 14 child particles predicted by the Apollonian packing model. This deviation strongly supports the presence of multistage breakage processes in the numerical simulations, wherein parent particles undergo not only primary breakage but also secondary and even tertiary fragmentation. From a micromechanical perspective, this finding verifies the unique advantage of the Fragment Replacement Method (FRM) in simulating the continuous breakage behavior of granular materials. The realization of multilevel breakage overcomes the limitations of conventional single-breakage models, enabling more realistic simulation of the progressive fragmentation process in geomaterials.

By extracting the relative breakage ratio (B_r) of the numerical specimens under different strain levels and combining the data from Table 5 and Fig.11, the relationship

curves of cumulative child particle generation and parent particle breakage versus axial strain under different gradation conditions are plotted, as shown in Fig. 12.

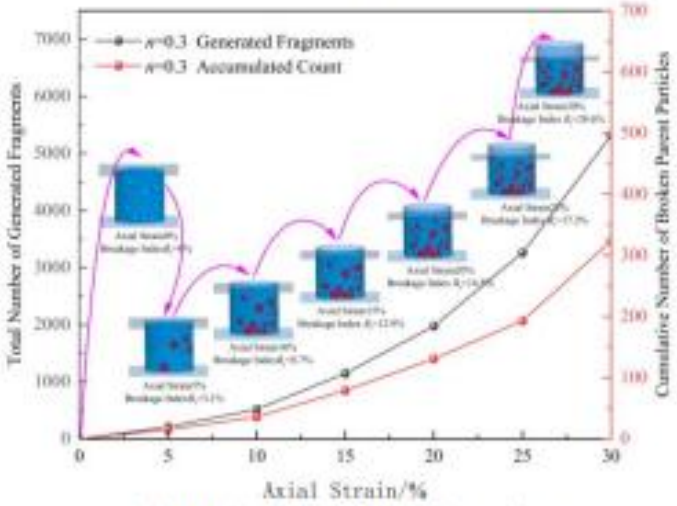

（a）A1-1 Numerical model specimen

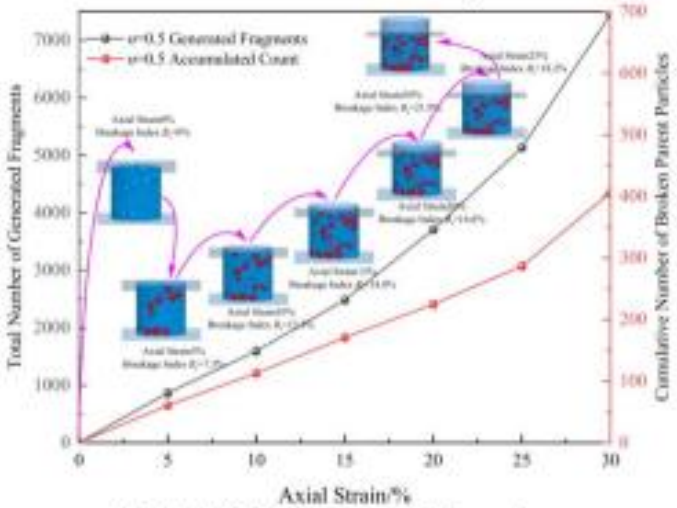

（b）A2-2 Numerical model specimen

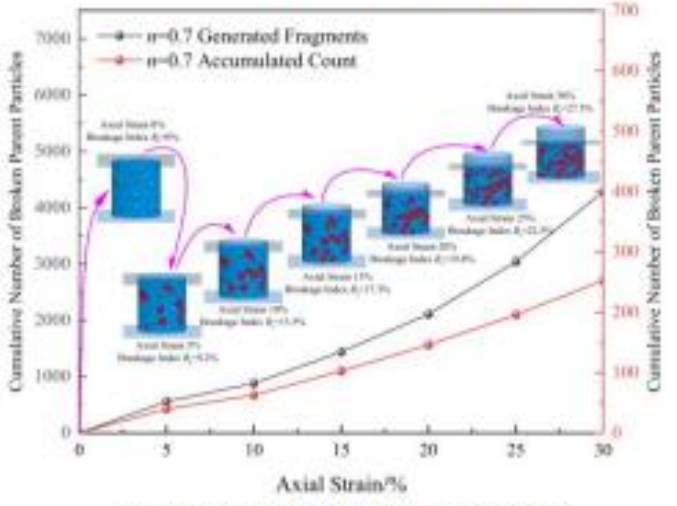

（c）A3-3 Numerical model specimen

Fig. 12 Evolution of fragment-to-parent particle ratio under increasing axial strain

From Fig. 12, it can be observed that the relative breakage rate (B_r) of numerical specimens A1-1, A2-2, and A3-3 increases with axial strain. When the axial strain reaches 30%, the relative breakage rates of specimens A1-1, A2-2, and A3-3 are 20.6%, 21.9%, and 27.5%, respectively. In comparison, the corresponding relative breakage rates of the laboratory-tested specimens A1, A2, and A3 reported in Section 3.2.4 are 28.37%, 30.01%, and 33.62%.

Considering both the numerical simulations and the laboratory experiments, the relative breakage rate B_r of phyllite rockfill specimens under triaxial compression exhibits a positive correlation with the Talbot gradation index n. The results of the numerical simulations are qualitatively consistent with those of the physical experiments.

Since the particle breakage process of phyllite rockfill aggregates under external loading is a highly complex mechanical phenomenon, it is unrealistic for numerical models to fully replicate the actual test process at a 1:1 scale. Nevertheless, the stress–strain curves obtained from the simulations exhibit a high degree of agreement with those from laboratory tests. Furthermore, the qualitative analysis of breakage evolution in this section aligns well with experimental observations, indicating that the simulation results are highly reliable and can provide valuable support for subsequent studies.

Moreover, as shown in Fig. 12, the slope of the curve-which represents the cumulative number of generated fragments with increasing axial strain-varies significantly across different loading stages. This phenomenon can be attributed to the

varying severity of particle breakage within the specimens at different deformation stages. To further investigate this behavior, a growth rate formula is introduced for in-depth analysis, as shown in Equation (19):

$$v_i = \frac{N_i - N_{i-1}}{N_{i-1}} \tag{19}$$

Where v_i represents the growth rate of generated fragments at axial strain level i; N_i denotes the cumulative number of generated child particles at strain level i; and N_{i-1} is the cumulative number at the previous strain level $i-1$.

Based on Equation (19), the growth rate of cumulative fragment generation during different loading stages was calculated for each specimen. The results are illustrated in Fig.13.

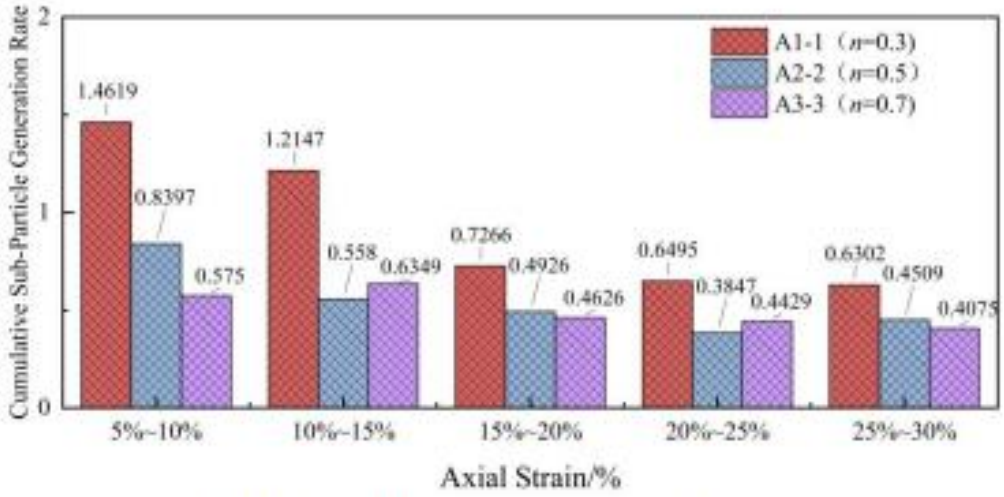

Fig.13 Variation of fragment growth rate with axial strain

As shown in Fig.13, during the axial strain intervals of 5%–10% and 10%–15%, the fragment growth rates of numerical specimens A1-1, A2-2, and A3-3 are 1.4619, 0.8379, 0.575 and 1.2147, 0.558, and 0.6349, respectively. These values are significantly higher than the corresponding growth rates observed during the 15%–30% strain stage for each specimen.

This trend is attributed to the fact that the 5%–15% axial strain range corresponds to the rapid deformation phase on the stress–strain curve. In this stage, the internal particles of the specimen undergo rapid rearrangement under external loading, adapting to the state of stress through positional adjustments and intense particle breakage. As a result, the rate of fragment generation is relatively high.

By contrast, the 15%–30% axial strain stage aligns with the slow or steady deformation phase of the stress–strain curve, during which axial strain increases more gradually. Consequently, the intensity of particle rearrangement decreases, leading to lower breakage activity and thus a reduced fragment growth rate.

4. Conclusion

This study focuses on phyllite construction waste generated during road development in the Longnan region of Gansu Province. Based on its fundamental engineering properties, a series of laboratory tests were conducted to investigate the mechanical and crushing behaviors of both single particles and particle assemblies. In addition, a discrete element model of continuously graded phyllite was developed using PFC3D to simulate particle breakage behavior. From both macroscopic and mesoscopic perspectives, the dynamic evolution of particle crushing and its underlying mechanisms were analyzed. The main findings and conclusions are summarized as follows:

(1) Phyllite is mainly composed of muscovite (38%), orthoclase (27.1%), kaolinite (22.5%), and quartz (12.4%), categorizing it as a moderately weathered soft rock. SEM

leading to water-induced disintegration and strength degradation through exfoliation.

(2) Single-particle compression tests showed that strength follows a Weibull distribution. The Weibull modulus decreased with increasing particle size, indicating greater variability in strength for larger particles. Additionally, crushing strength decreased as particle size and loading height increased, demonstrating a size effect.

(3) Confined compression tests revealed a three-stage stress–strain curve. Continuously graded specimens exhibited better resistance to deformation than single-sized specimens. The breakage ratio showed a negative correlation with both the Talbot index and particle size, with larger particles (10–31.5 mm) experiencing more crushing. A Talbot index of 0.5 provided optimal performance for subgrade fill applications.

(4) A discrete element model incorporating FRM and Weibull-based crushing thresholds accurately simulated stress–strain behavior and breakage patterns. It effectively captured multistage particle fragmentation, showing that a Talbot index of ~0.5 optimizes gradation and crushing resistance in phyllite material, offering insights into utilizing soft rock waste for subgrade fill and guiding discrete element model calibration.

Acknowledgement

This work was supported by the National Natural Science Foundation of China (Grant Nos. 52268058 and W2421075), the Royal Society–NFSC Project (ICE/NFSC/242496), the Key Research and Development Project of Lanzhou Jiaotong

University (LZJTU-ZDYF2305), the Gansu Provincial Department of Education Industrial Support Program Project, China (2023CYZC-34)

Declaration of Competing Interest

The authors declare that they have no known competing financial interests or personal relationships that could have appeared to influence the work reported in this paper.

References

Hiramatsu, Y., & Oka, Y. (1966). Determination of the tensile strength of rock by a compression test of an irregular test piece. Proceedings of the International Journal of Rock Mechanics and Mining Sciences & Geomechanics Abstracts, F. Elsevier.

Nakata, Y., Hyde, A. F. L., & Hyodo, M. (1999). A probabilistic approach to sand particle crushing in the triaxial test. Géotechnique, 49(5), 567-583.

McDowell, G. R., & Bolton, M. D. (1998). On the micromechanics of crushable aggregates. Géotechnique, 48(5), 667–679.

Lim, W. L., & McDowell, G. R. (2005). Discrete element modelling of railway ballast. Granular Matter, 7(1), 19–29.

Ovalle, C., Reyes, O., Lizcano, A., & Paredes, J. (2015). Weibull statistics applied to the tensile strength variability of heterogeneous rocks. Engineering Geology, 185, 55–63.

Kuang, D., Wang, Q., Zhang, X., et al. (2023). DEM analysis of single particle crushing considering the inhomogeneity of material properties. Powder Technology, 416, 118190.

Zhang, C., Wang, S., Jin, Y., et al. (2024). Discrete element method simulation of granular materials considering particle breakage in geotechnical and mining engineering: A short review. Powder Technology, 429, 118480.

Rotter, T., Osei-Agyemang, M., & Zhang, L. (2024). Improving BPM for brittle particle simulation: Multi-scale bonding optimization. Granular Matter, 26(2), 35.

Gao, Y., Huang, Y., & Chen, Z. (2023). Particle breakage characteristics of loess under isotropic compression at different stress levels. Engineering Geology, 319, 107112.

Jia, T., Luo, Y., & Wang, X. (2022). Experimental study on particle breakage of basalt aggregates

under different stress paths. Rock and Soil Mechanics, 43(8), 2189–2201. (in Chinese)

Zhang, F., Hu, D., Xie, S., & Shao, J. (2020). Weakening mechanisms of phyllite under hydration–drying cycles. Engineering Geology, 264, 105394.

Wang, J., Chi, S., Yan, S., et al. (2023). Representative elementary volume for characterizing mechanical parameters of scaled gradation rockfill materials in laboratory tests. Journal of Zhejiang University: Engineering Science, 57, 1418–1427.

Xu, J., Zhang, J., Huang, Y., et al. (2011). Experimental study and application on compaction and deformation characteristics of gangue–fly ash backfill in fully mechanized mining. Journal of Mining and Safety Engineering, 28(01), 158–162.

Jaeger, J. C. (1967). Failure of rocks under tensile conditions. International Journal of Rock Mechanics and Mining Sciences & Geomechanics Abstracts, 4(2), 219–227.

Lobo-Guerrero, S., & Vallejo, L. E. (2006). Application of Weibull statistics to the tensile strength of rock aggregates. Journal of Geotechnical and Geoenvironmental Engineering, 132(6), 786–790.

Weibull, W. (1951). A statistical distribution function of wide applicability. Journal of Applied Mechanics, 18, 293–297.

Zhang, Y., Buscarnera, G., & Einav, I. (2016). Grain size dependence of yielding in granular soils interpreted using fracture mechanics, breakage mechanics and Weibull statistics. Géotechnique, 66(2), 149–160.

Meng, M., Yuan, Z., & Jiang, X. (2022). Experimental study on single-particle crushing, strength, and size effect of calcareous sand–quartz sand. Science China, 52.

Cai, P., Mao, X., Liu, Y., et al. (2025). Study on single-particle crushing, strength, size and morphology effects of recycled fill materials. China Journal of Highway and Transport, 2025-03-10.

Cao, J., & Wang, Z. (2005). Experimental study on continuously graded crushed stone materials. Highway Engineering, 14–16, 20.

Hardin, B. O. (1985). Crushing of soil particles. Journal of Geotechnical Engineering, 111(10), 1177–1192.

Zhang, K., Zhang, S., Teng, J., et al. (2017). Three-dimensional discrete element simulation study

on particle breakage. Rock and Soil Mechanics, 38, 2119–2127.

Xu, S., Xu, J., Xu, C., et al. (2024). Discrete element analysis of the influence of particle breakage on the macro- and micromechanical properties of hydrate-bearing sediment matrix. Acta Energiae Solaris Sinica, 45, 680–690.

Tapias, M., Gili, J., & Alonso, E. E. (2012). Scale effects in rockfill behaviour. Géotechnique Letters, 2, 155–160.

Ciantia, M. O., Arroyo, M., Calvetti, F., et al. (2015). An approach to enhance efficiency of DEM modelling of soils with crushable grains. Géotechnique, 65(2), 91–110.

Åström, J. A., & Herrmann, H. J. (1998). Fragmentation of grains in a two-dimensional packing. The European Physical Journal B-Condensed Matter and Complex Systems, 5(3), 551–554.

McDowell, G. R., & De Bono, J. P. (2013). On the micromechanics of one-dimensional normal compression. Géotechnique, 63(11), 895–908.

Bono, J. D., & McDowell, G. R. (2014). DEM of triaxial tests on crushable sand.

Baant, Z. P. (1984). Size effect in blunt fracture: Concrete, rock, metal. Journal of Engineering Mechanics, 110(4), 518–535.